Tsukuba Geoenvironmental Sciences, Vol. 16, pp. 15-25, Dec. 25, 2020

Geomorphological features of shallow landslides in hillslopes underlain by mixed rock of sandstone and mudstone: A case of heavy rainfall on August 20, 2014 in Hiroshima City, Japan

Naoyuki YOSHIHARA[a*], Tsuyoshi HATTANJI[b], Shoji DOSHIDA[c], Yasushi TANAKA[d] and Takahisa FURUICHI[e]

Abstract

Shallow landslides occurred due to heavy rainfall on August 20, 2014 in Hiroshima City, southwest Japan. The topographic analysis with high resolution digital elevation models (DEMs) revealed that (1) many landslides occurred at slopes steeper than 30°, and (2) specific source areas of the landslide scarps in the mixed-rock area were larger than those in the granite area by one to two orders of magnitude. Field observations revealed that the types of landslides were mainly divided into planar translational and V-shaped. Some of them in the mixed-rock area formed deeper scars (6 m maximum) than those in the granite area. Soil samples collected from the scarps in the mixed-rock area showed lower hydraulic conductivity than those in the granite area and showed a grain-size distribution with high clay content ranging from 16.8%–51.7%. The infinite slope stability analysis indicated that some planar-translational landslides in the mixed-rock area could have occurred when the soil layers reached nearly full saturation. Saturation of soil layer and groundwater flow due to large specific source areas possibly caused the shallow landslides in the mixed rock area.

Key words: GIS, Specific source area, Soil property, Infinite slope stability analysis, Groundwater flow

1. Introduction

Shallow landslides triggered by heavy rainfall occur on steep soil-mantled hillslopes. Landslide masses suddenly move down as debris flows and occasionally cause disasters (Iverson, 2000). A heavy rainfall event on August 20, 2014 caused shallow landslides on hillslopes in the northern part of Hiroshima City, southwestern Japan. Some papers reported the results of field observations and stability analyses for shallow landslides, and they discussed the triggering mechanisms based on geological, meteorological, and geomorphological conditions (e.g., Kaibori *et al*., 2014; Matsushi *et al*., 2015; Saito *et al*., 2015; Watakabe and Matsushi, 2019). One of the characteristics of this event is that landslides and debris flows occurred in headwater basins underlain by various rocks including granite, rhyolite dikes, schist, and mixed rocks of sandstone and mudstone (Saito *et al*., 2015). In particular, shallow landslides in mixed-rock areas rarely occurred. Therefore, additional surveys are essential for understanding landslide disasters in mixed-rock areas.

This study reveals the characteristics of shallow landslides induced by the heavy rainfall in Hiroshima City on August 20, 2014 from the perspective of geology, topography, and the physical properties of the soil. In particular, we focus on the topographic characteristics and triggering conditions of landslides in hillslopes underlain by mixed rock.

2. Site description

Figure 1 shows the slope map, elevation changes, and geological boundaries around Mt. Abu (586 m asl.). The northern part of Mt. Abu is composed of Jurassic schist and Jurassic mixed rock of mudstone, sandstone, and chert (Saito *et al*., 2015). The mixed rock is weakly metamorphosed. Late Cretaceous granite exposes in the southern part (Takahashi, 1991; Saito *et al*., 2015). Late Cretaceous rhyolite dike intruded between the mixed-rock and granite areas. The mean annual precipitation is 1690 mm, and the mean temperature is 14.8°C at the Japan Meteorological Agency station, Miiri, about 5 km north from Mt. Abu. Planted forest of cedar and cypress occupies the northern slope. Oak and pine are in most of the other areas.

During heavy rainfall from August 19 to 20, 2014, the maximum amounts of 1-, 3-, and 24-hour rainfall were

[a] Graduate School of Life and Environmental Sciences, currently Geological Survey of Japan, National Institute of Advanced Industrial Science and Technology
[b] Faculty of Life and Environmental Sciences, University of Tsukuba
[c] National Research Institute of Fire and Disaster
[d] Department of Geography, Komazawa University
[e] Forestry and Forest Products Research Institute
[*] Corresponding author*: Naoyuki Yoshihara: Geological Survey of Japan, National Institute of Advanced Industrial Science and Technology, Central 7, 1-1-1, Higashi, Tsukuba, Ibaraki, 305-8567, Japan.

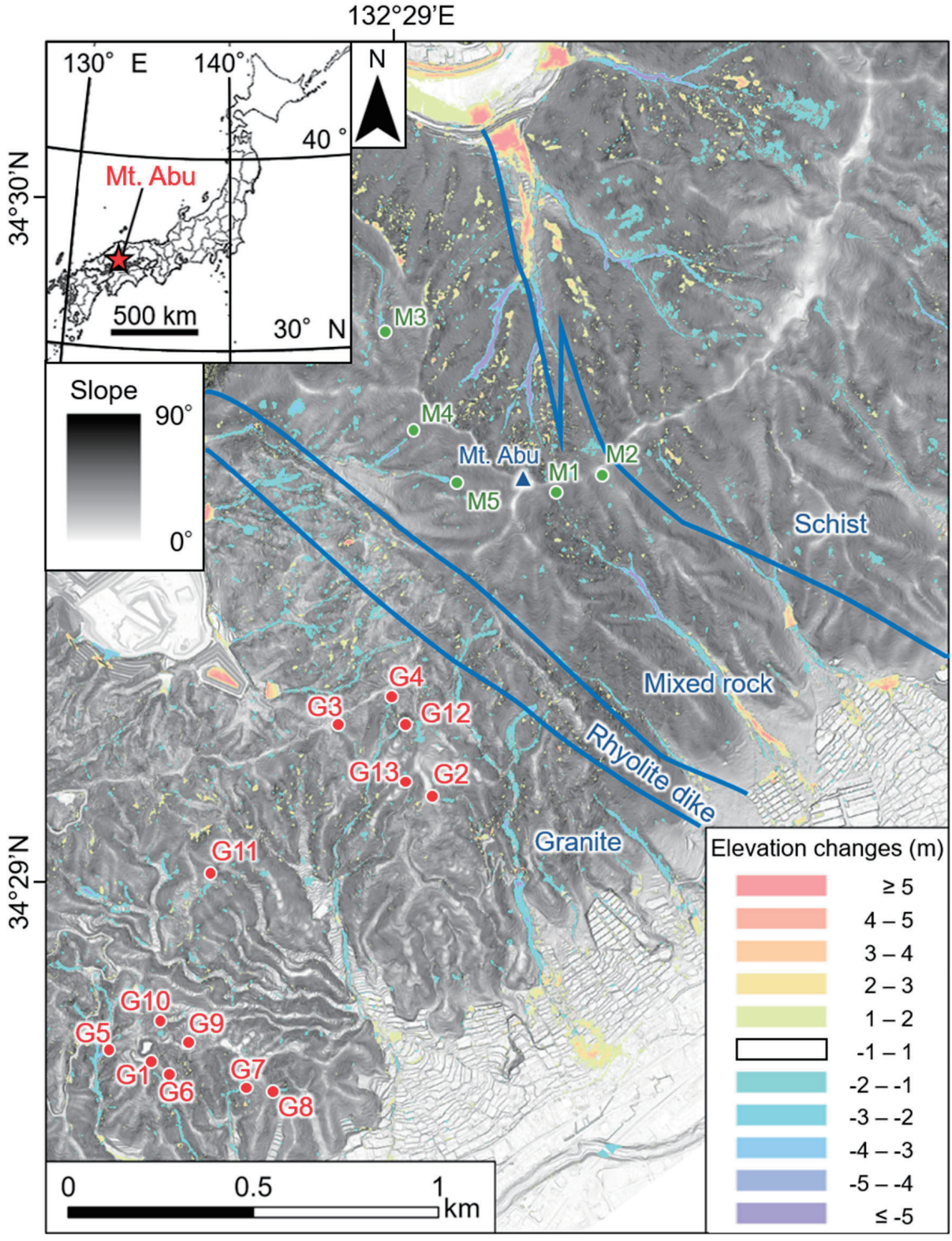

Fig. 1 Slope map with elevation changes between 2009 and 2014. The closed circles represent landslides for field survey. The blue lines indicate geological boundaries. Elevation changes larger than 1 m are shown in accordance with the color scale.

101.0, 217.5, and 257.0 mm, respectively, at the Japan Meteorological Agency station, Miiri. These values were the highest on record from 2001 to 2014. Shallow landslides occurred concurrently when the maximum 1-hour rainfall intensity exceeded 70 mm, and the maximum 3-hour rainfall was more than 160–180 mm (Matsushi *et al*., 2015).

3. Method

3.1. GIS-based topographic analysis

We measured the elevation changes, slope angles, widths, and specific source areas of the landslides using ArcMap ver. 10.6 (ESRI Inc.) Two digital elevation models with 1-m resolution (hereafter 1-m DEMs) taken in 2009 (before the disaster) and 2014 (after the disaster) are the base maps for the topographic analyses. The elevation changes are the subtraction of elevations in 2009 from those in 2014. We determined landslides from the elevation changes and landslide scars seen in aerial photographs taken by the Geospatial Information Authority of Japan. The slope angle of each landslide is the mean angle along the longitudinal line ranging from 6.6 to 14.9 m toward the maximum slope direction. A specific source area of a landslide scarp, A/B, is the size of the upslope source area above the scarp, A, divided by the width of the landslide, B. The number of measured landslides was 23 for the mixed-rock area and 31 for the granite area.

3.2. Field survey

We conducted a field survey at 18 landslide scars, M1–M5 in the mixed-rock area and G1–G13 in the granite area (Fig. 1) and classified the shape of these landslides into planar-translational type or V-shaped type with the 1-m DEMs. The depth profile of soil hardness (SH) was measured using a Yamanaka-type soil hardness tester (Daiki corp. Japan) at the scarps of seven landslides (M1–M5, G1 and G2). The scarps were vertically planarized before measuring the SH. Then, undisturbed soil samples of 100 mL were cored from the scarps at every 20–55 cm depth interval, except for two samples taken from a deeper zone of M5. The sample cores were 5.0 cm in diameter and 5.1 cm high. In addition, undisturbed samples for the direct shear test were collected from the depths of the sliding surface of M3 and G2 using a trimming ring 6.0 cm in diameter and 2.0 cm high.

A cone penetration test was conducted at 1 m upslope from each sampling site of the east and west blocks of M3 and the north block of M4. The cone penetrometer (Tsukuba Maruto, Japan) is composed of a 2.5-cm diameter cone with a 60° tip, a 1.6-cm diameter rod, and a 5-kg hammer. The rod was vertically penetrated into the ground by the impact of the hammer falling 50 cm. The cone penetration resistance, Nc, is the number of hammer drops required for 10-cm penetration of the rod. In general, the Nc of granitic bedrock is regarded to be more than 30 (Ohsaka *et al*., 1992; Wakatsuki and Matsukura, 2008; Yamashita *et al*., 2017; Watakabe and Matsushi, 2019). The bedrock surface at our study sites was defined as the depth where Nc exceeded 30.

3.3. Laboratory experiments

We measured the dry bulk density, specific gravity of soil, porosity, water saturation, grain-size distribution, and saturated hydraulic conductivity (K) of the cored samples of 100-mL volume. Dry bulk densities of each 100-mL sample were measured after oven drying at 110°C for 24 hr. Specific gravities of soil were measured using a pycnometer. Porosities were calculated from the dry bulk density and the specific gravity of the soil. Water saturations at natural water content were calculated from the dry bulk density, the specific gravity of the soil, and the soil water content. The grain-size distribution was measured by sieving for coarser grains (>0.074 mm) and by using a sedimentation method with a settling tube for finer grains (≤0.074 mm). Colloids were dispersed using sodium hexametaphosphate prior to the sedimentation analysis. The hydraulic conductivity, K, was measured with a permeability tester (DIK-4050, Daiki corp. Japan).

The shear strength (cohesion and angle of shearing resistance) of the undisturbed soil samples was measured with a direct shear tester (Tsukuba Maruto, Japan). During this test, the moisture of the soil cores was adjusted to natural or capillary saturated condition. Displacement rate was 1 mm/min, and normal stresses were 100, 200, 300, and 400 gf/cm^2.

4. Results

4.1. Topographic features

Landslides in the mixed-rock area formed deeper scars than those in the granite area (Fig. 1). Elevation change of landslide scars indicating more than 2 m had the majority in the mixed-rock area. Landslide scars in the granite area showed approximately 1 m of erosion.

The specific source areas of landslide scarps, A/B, are plotted against the local slopes at landslide scarps in the mixed-rock area and the granite area (Fig. 2). The landslides in the mixed-rock area required specific source areas of more than 10^2 m. The specific source areas were clearly larger than those in the granite area.

Most landslides occurred at slopes steeper than 30° ($\tan\theta = 0.58$) for both areas. Although the mean slope angle of landslides in the mixed-rock area (37.8°, $\tan\theta = 0.78$,

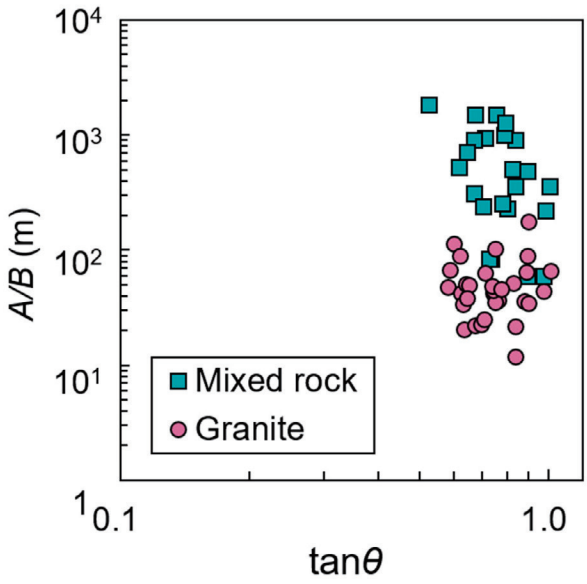

Fig. 2 Specific source areas (A/B) plotted against local slope ($\tan\theta$) of landslides.

Table 1 Classification of investigated landslides.

Site	Type
Mixed rock (Sandstone and mudstone)	
M1	Planar translational
M2	Planar translational
M3 (East block)	Planar translational
M3 (West block)	V-shaped
M4 (North block)	Planar translational
M4 (South block)	V-shaped
M5	V-shaped
Granite	
G1	Planar translational
G2	Planar translational
G3	Planar translational
G4	Planar translational
G5	V-shaped
G6	Planar translational
G7	Planar translational
G8	Planar translational
G9	Planar translational
G10	Planar translational
G11	Planar translational
G12	Planar translational
G13	Planar translational

N = 23) was slightly larger than that of the granite area (36.8°, $\tan\theta = 0.75$, N = 31), the difference was not statistically significant ($p > 0.05$).

4.2. Classification of landslides

Figure 3 shows the photographs of the 18 investigated landslides (M1–M5 and G1–G13). These landslides were divided into two types, i.e., (1) planar translational type and (2) V-shaped type (Table 1).

Landslides M1 and M2 corresponded to planar translational landslides (Figs. 3a and 3b). Their depths were approximately 1.0 m. The shallow landslide M1 had a 2.8-m width, a 485-m specific source area, and a slope of 41.7° ($\tan\theta = 0.89$). The shallow landslide M2 occurred on a slope of 35.9° ($\tan\theta = 0.72$), and the width was 14.4 m. The specific source area of M2 was 84 m.

Landslides M3 and M4 had complex structures, both of which were composed of two blocks. In M3, an east-side planar translational landslide adjoined a west-side V-shaped landslide (Fig. 3c). The depth, width, and slope angle were 2.0 m, 10.2 m, and 33.9° ($\tan\theta = 0.67$) for the planar translational landslide block, respectively. The V-shaped landslide block had a 3.5-m depth, 8.4-m width, and 27.7° ($\tan\theta = 0.53$) slope angle. The scarp of the adjoining V-shaped landslide was located 10 m upslope from the scarp of the planar translational landslide. Groundwater seeps at the bottom of the V-shaped landslide scar in M3. The south block of M4 (Fig. 3d) was a V-shaped landslide 6.0 m deep and 14.8 m wide. This block of the landslide connected to the north block with a smaller landslide scar 1.8 m deep and 6.7 m wide (Fig. 3e).

Landslide M5 was a V-shaped one with a deeper (approximately 6.0 m) and wider (18.2 m) scar than the other sites (Fig. 3f). The slope angle of the sliding surface was 33.8° ($\tan\theta = 0.67$). Groundwater seeps below the scarp of M5 (Fig. 3g). Bedrock was exposed at the bottom of the valley where subsequent rainfall and/or groundwater seepage was supposed to erode the overlying debris on the landslide scar.

Landslides of G1–G2 were classified as planar translational type (Figs. 3h and 3i). These landslides had similar topographic features. The landslides had sliding surfaces about 1 m deep. The widths and slope angles of G1 were 8.5 m and 38.0° ($\tan\theta = 0.78$), and those of G2 were 9.6 m and 35.6° ($\tan\theta = 0.72$). These values were typical for shallow landslides on granitic hillslopes. Topographic types of G3–G13 were also clearly identified from the photographs (Fig. 3) and the elevation changes of the 1-m DEMs (Fig. 1). We could find only one V-shaped landslide (G5) through our field survey.

Fig. 3 Photographs of investigated sites in the mixed-rock area (a–g) and in the granite area (h–t). The depths of the sliding surface are included in the photographs in which detailed surveys were conducted. Two landslides were adjoined in each of M3 and M4 (c-e). Seepage in (g) was found at the downslope of M5 (f).

4.3. Soil properties

Table 2 shows the dry bulk density, porosity, water saturation, and specific gravity of soil samples. The soil properties in each site indicated (1) the smaller dry bulk density at shallower soil layers, (2) the relatively higher porosity of M1–M5 than G1 and G2, and (3) the higher water saturation of the soil layer deeper than 100 cm.

Figure 4 shows the grain-size distribution for soil samples of the east block of M3, the north block of M4, and M5. The clay and silt contents of four samples extracted from deeper zone of the scar of M5 were combined because these samples were not dispersed enough in this experimental procedure. For the case of M3, the clay content was less than 27.2% for the shallower layer (≤0.75 m) and more than 33.0% for the deeper layer (≥1.45 m, Fig. 4a). The silt content of the three shallow samples (30, 55, and 75 cm in depth) indicated slightly higher values than the other three samples. All samples of M3 contained some gravel (>2 mm in diameter). The deeper two samples were clay-rich soil with high porosity and water saturation (Table 2). The clay content of M4 generally increased with depth, whereas no noticeable difference was found in the contents of sand and gravel (Fig. 4b). The total contents of clay and silt of M5 increased as the depth increased from 20 to 300 cm and decreased thereunder (Fig. 4c). For samples of M5, gravel occupied 21.3% and 38.8% of the content at 370 cm and 650 cm deep, respectively.

Table 2 Physical properties of soil samples.

Site	Depth (cm)	Dry bulk density (g/cm^3)	Porosity (%)	Water saturation (%)	Specific gravity of soil (g/cm^3)
M1	25	0.70	74.2	40.3	2.72
	50	0.81	70.2	51.4	
	75	0.91	66.3	53.4	
	100	0.97	64.4	53.9	
M2	40	0.80	70.8	44.8	2.73
	60	0.82	70.0	45.2	
	80	0.94	65.5	55.3	
	100	1.17	57.0	78.2	
	120	1.30	52.4	78.0	
M3 (East block)	30	1.00	63.4	55.7	2.74
	55	1.12	59.2	70.8	
	75	1.03	62.4	57.9	
	145	1.26	54.0	71.6	
	195	1.44	47.4	95.0	
	220	1.39	49.0	97.5	
M4 (North block)	30	0.83	68.8	38.0	2.65
	50	0.81	69.6	36.4	
	70	0.82	69.3	37.5	
	95	1.11	58.3	61.0	
	120	1.09	58.8	67.6	
	145	1.20	54.8	66.6	
	165	1.12	57.9	62.5	
M5	20	0.90	67.2	51.5	2.74
	50	0.80	70.9	42.2	
	95	1.05	61.7	59.4	
	150	1.23	55.0	70.0	
	200	1.31	52.2	79.4	
	300	1.13	58.6	60.5	
	370	1.19	56.6	60.1	
	650	1.41	48.3	61.1	
G1	20	1.10	58.0	23.2	2.63
	40	1.17	55.4	29.4	
	60	1.33	49.6	38.3	
	80	1.47	44.0	37.1	
	100	1.49	43.5	48.0	
G2	20	1.17	55.7	33.4	2.64
	40	1.28	51.6	39.7	
	60	1.25	52.6	35.2	
	80	1.55	41.4	49.9	

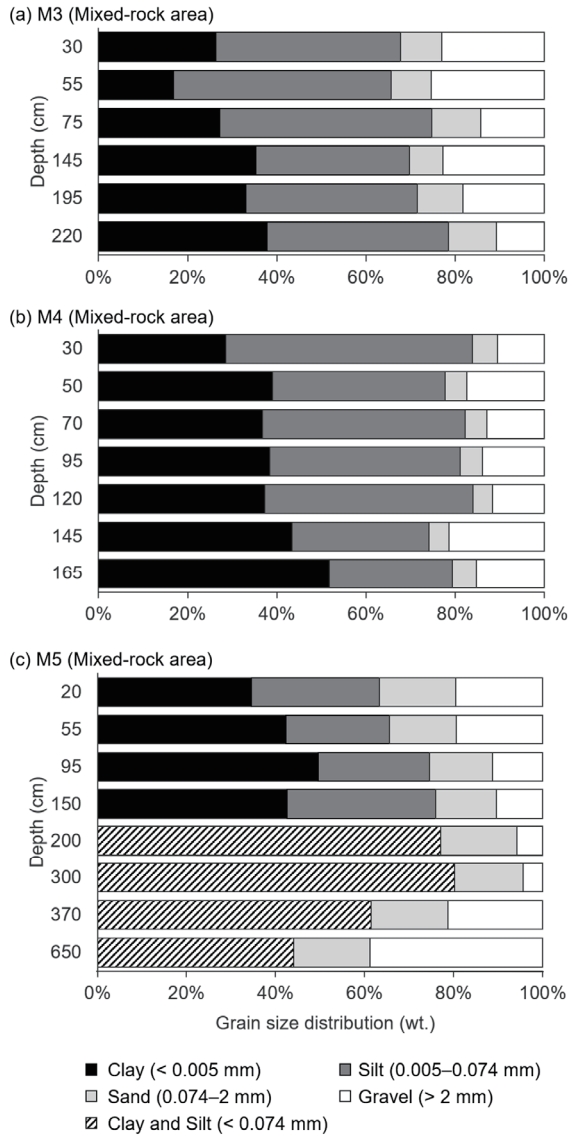

Fig. 4 Grain-size distribution of soil samples collected from landslide scarps of the east block of M3 (a), the north block of M4 (b), and M5 (c). The percentage contents of clay and silt for the deeper four samples in M5 were combined because these samples were not dispersed enough in the experimental procedure.

Figure 5 shows the vertical profiles of an *Nc* at three landslide scarps. The bedrock surface was defined as the depth where *Nc* exceeded 30. The sliding surface of the east block of M3 was in the clay-rich layer overlying the bedrock (Fig. 5a). Figure 5b exhibits the closeness between the sliding surface and the bedrock surface at the scarp of the west block of M3. The *Nc* profile at the north block of M4 indicated the sliding surface did not correspond with the bedrock surface (Fig. 5c).

Figure 6 shows the profiles of *SH* and *K* with the estimated depths of the sliding surface. The measurement of *SH* was omitted for G1 and G2. In M1, the low-*SH* (5.2 – 15.8 mm) and high-*K* (3.0×10^{-2} – 8.7×10^{-2} cm/s) soil layer overlaid the sliding surface at 1.0-m depth. This sliding surface was identical to the soil-bedrock interface. The sliding surfaces of M2 and the east block of M3 were located around the top of the impermeable clay-rich layers (8.0×10^{-7} – 1.9×10^{-6} cm/s). In M4, the *SH* generally decreased as the depth increased from 50 to 200 cm, and the *K* changed within a range of 10^{-4} – 10^{-1} cm/s, even around the sliding surface. In M5, the thick soil layer containing gravel indicated an intermediate *SH* (8.0 – 20.3 mm) and high *K* (3.9×10^{-4} – 6.5×10^{-2} cm/s) compared to the other sites. In G1 and G2, the *K* ranged from 8.0×10^{-2} to 1.0×10^{-1} cm/s, and the sliding surfaces were consistent with the soil-bedrock interfaces. Except for the impermeable clay-rich layers in M2 and the east block of M3, the soil layer 95 and 145 cm deep in the north block of M4, and the soil layer 200 cm deep in M5, the values of *K* were high, indicating more than 10^{-3} cm/s.

Figure 7 shows the shear strength of the sliding surface of a planar translational landslide of M3 and G2. The cohesion of the soil samples substantially changed depending on the conditions of water saturation, whereas the angle of shearing resistance showed a little change. The saturated samples in M3 indicated a cohesion of 44.8 gf/cm^2, which was less than half for the natural samples of 114.9 gf/cm^2. The angles of shearing resistance were

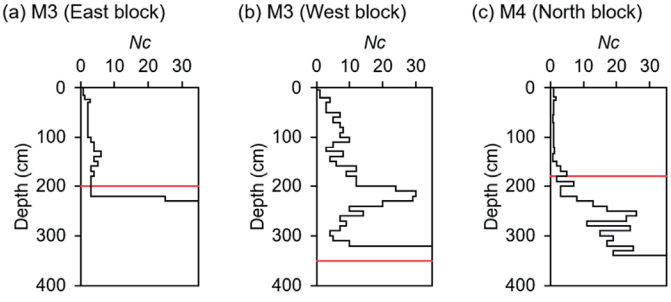

Fig. 5 Depth profiles of *Nc* at 1 m upslope from each sampling site in the mixed-rock area. (a) The east block of M3. (b) The west block of M3. (c) The north block of M4. The red line indicates the depth of the sliding surface estimated from field observations.

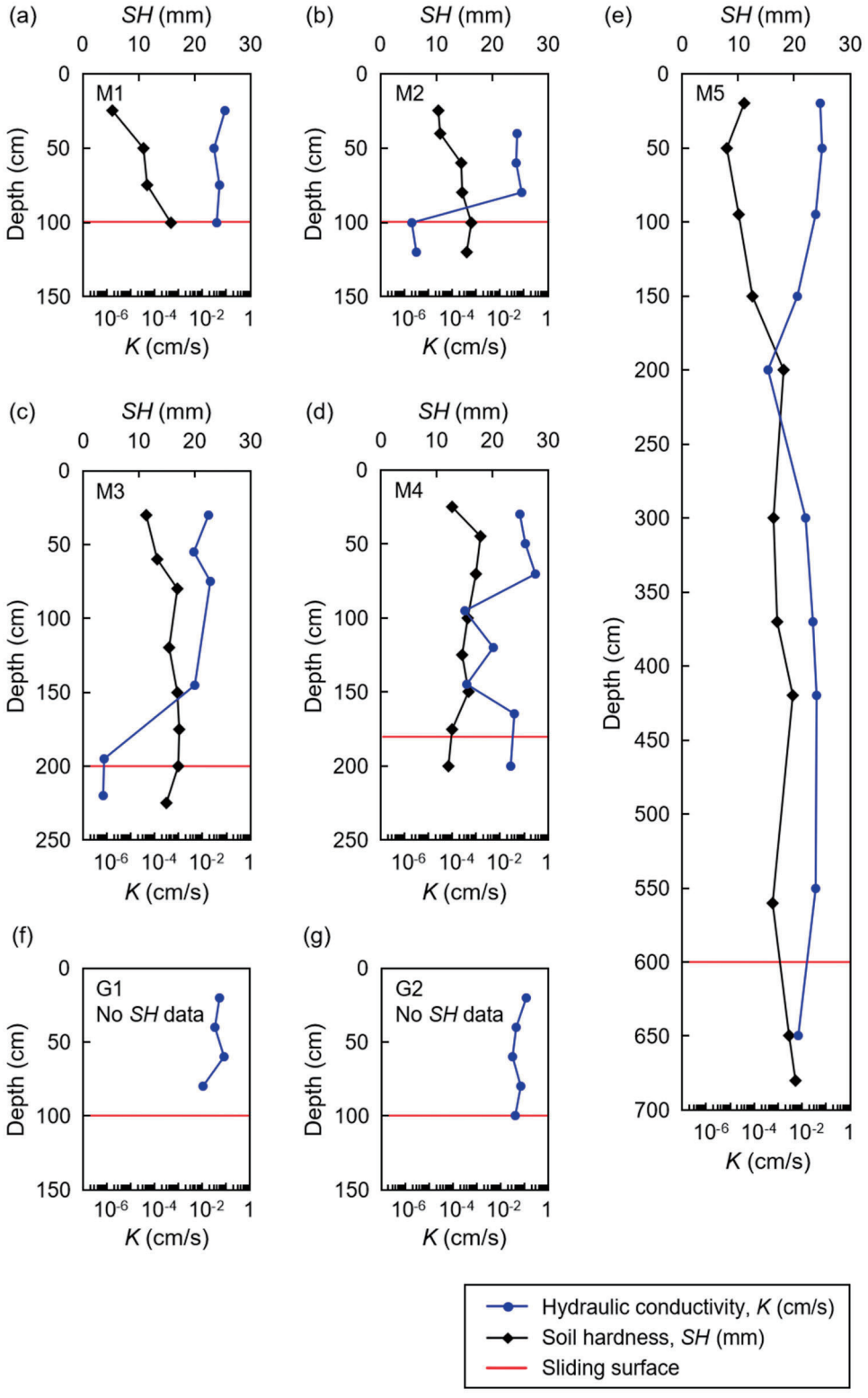

Fig. 6 Depth profiles of hydraulic conductivity (*K*), soil hardness (*SH*) and the depths of sliding surface in M1 (a), M2 (b), the east block of M3 (c), the north block of M4 (d), M5 (e), G1 (f) and G2 (g). The measurements of *SH* in G1 and G2 were omitted. The sliding surface was estimated based on in-field observations and the profiles of *K* and *SH*.

Table 3 Parameters applied to the infinite slope stability analysis.

Site	Z (cm)	γ_s (gf/cm^2)	β (°)	c (gf/cm^2)	φ (°)
M3 (East block)	200	1.70	33.9	44.8	42.6
G2	100	1.82	35.5	33.5	44.8

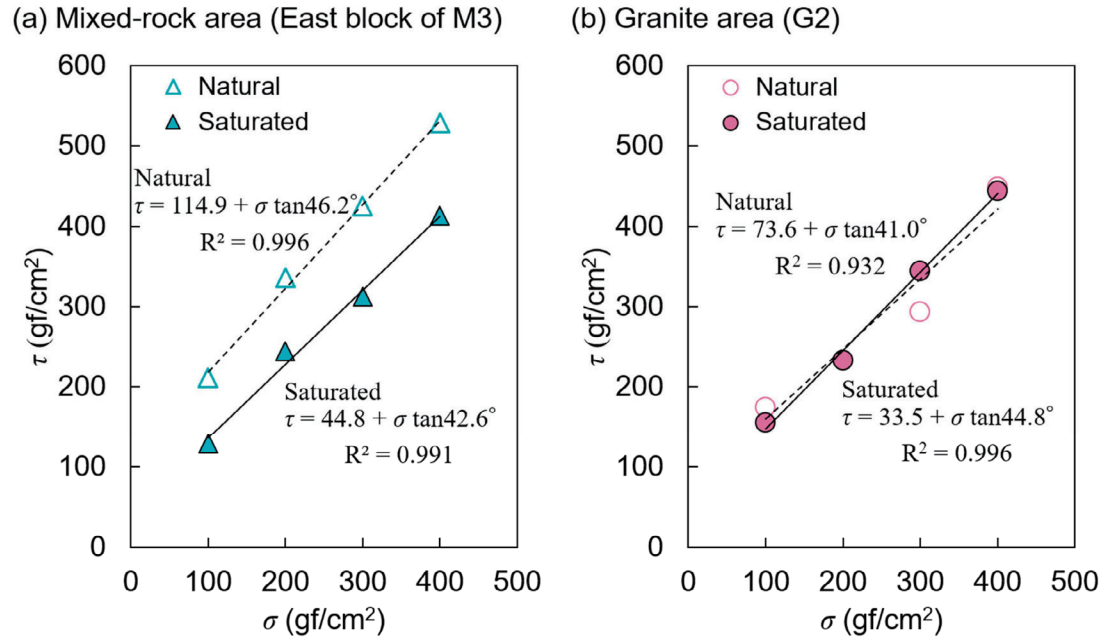

Fig. 7 Results of direct shear test of the east block of M3 (a) and G2 (b). The test was conducted using undisturbed soil samples under the natural or capillary-saturated conditions. The sample was collected from sliding surface in each landslide.

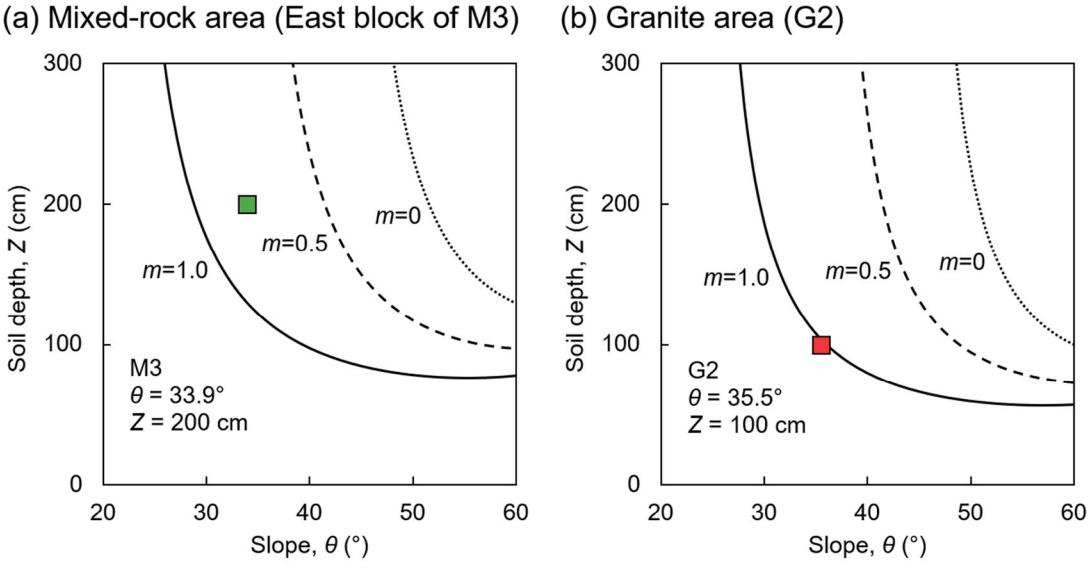

Fig. 8 Slope stability analyses of the east block of M3 (a) and G2 (b). The lines in the figure indicate the critical conditions of the slope (F_s = 1). If m = 0, the groundwater table is assumed to be below the soil layer. If m = 1, the groundwater table correlates with the ground surface, indicating high saturation.

46.2° and 42.6° for the natural and saturated samples, respectively. The samples in G2 exhibited weaker cohesion compared to those of M3 at the same saturation degrees. The angles of shearing resistance ranged from 41.0° to 46.2° among all samples.

5. Discussion

Our data suggests that both planar-translational landslides and V-shaped landslides occurred in the mixed-rock area while planar-translational type predominated in the granite area. Large specific source areas exceeding 10^2 m for V-shaped type would facilitate supply of rainwater and groundwater to soil layers through several paths. Consequently, excessive supply of water might cause V-shaped landslides.

Major composition of sliding surface of planar translational type in the mixed-rock area were soil-bedrock interfaces or between permeability soil and impermeable clay-rich soil. Most of planar-translational landslides in the granite area occurred on soil-bedrock interfaces. These planar-translational landslides would occur by increment of saturation degree in the soil layers, but detailed triggering conditions have not discussed well, particularly for landslides in mixed-rock area. We thus estimated the triggering conditions of planar-translational landslides of M3 and G2 based on slope stability analysis.

We applied infinite slope stability analysis to specify the critical condition of G2 and the east block of M3, which were classified as planar-translational ones and had far longer sliding surfaces than the soil depths. Therefore, the infinite slope stability analysis was applicable to the two shallow landslides. We utilized the equation proposed by Skempton and DeLory (1957):

$$F_s = \frac{c + (\gamma_s - m\gamma_w) Z \cos^2\beta \tan\varphi}{\gamma_s Z \cos\beta \sin\beta} \quad (1)$$

where F_s is the factor of safety, γ_s is the unit weight of saturated soil (gf/cm^3), Z is the vertical soil thickness (m), β is the slope angle (°), φ is the angle of shearing resistance (°), c is the cohesion of soil (gf/cm^2), γ_w is the unit weight of water (gf/cm^3), and m is the parameter of the condition of groundwater level ranging from zero to one. A condition of $F_s < 1$ means that the soil-mantled hillslope is unstable. The groundwater table is below the sliding surface for $m = 0$, and it corresponds with the ground surface for $m = 1$. The parameters for Eq. (1) were obtained from topographic analysis and soil tests. Table 3 shows the parameters applied to Eq. (1). The unit weight of water (γ_w) is regarded to be 1.0 gf/cm^3.

Figure 8 illustrates the critical conditions of the G2 and east block of M3. Rectangles in this figure, which represent the values of the soil depth and slope angle of each landslide, were located around the zone of $F_s < 1$ for $m = 1$. This result means that the slopes became unstable when the soil layer reached nearly full saturation in both slopes. Considering the geometric similarity to the G2 and east block of M3, most of the other planar translational landslides in the study area likely occurred when the soil layer became nearly fully saturated. This estimation is consistent with other studies conducted in the schist area nearby where geological setting is the similar (Matsushi *et al*., 2015; Watakabe and Matsushi, 2019). Soil depths of the mixed-rock area exceeded 1 m, which were larger than common cases in the granite area. This thick soil layer contains much clay (Fig. 6c). Consequently, the impermeable clay-rich layer underlain by thick and cohesive soil layer must have caused the full saturation during the storm.

Although the infinite slope stability analysis could indicate the triggering conditions of planar translational landslides, the infinite slope stability analysis i.e., Eq. (1), is not applicable to the V-shaped landslide due to the complexities of shape and some presumable hydrological processes. Both field evidence and literature review imply the influence of groundwater on the triggering conditions of landslide in the mixed-rock area. Most of the landslides in the mixed-rock area required specific source areas of more than 10^2 m. Moreover, we also observed groundwater seepage at the scars of M5 and the west block of M3 during our field survey (Fig. 3). Mathewson *et al*. (1990) and Onda *et al*. (2001, 2004, 2006) demonstrated that rainfall frequently recharges into bedrock fractures and that the groundwater flow through the bedrock fractures is a significant controlling factor for runoff responses in mountainous regions underlain by sedimentary rocks. Matsushi *et al*. (2015) also suggested that the funnel-shaped landslides in the schist area, which are similar to V-shaped landslides, were influenced by groundwater. Larger source areas for landslide sites in the mixed-rock area may contribute to increases both in shallow subsurface flow and groundwater discharge and to a decrease in slope stability.

6. Conclusion

We classified shallow landslides that occurred on August 20, 2014 on Mt. Abu in the northern part of Hiroshima City in southwestern Japan into two types and estimated the critical conditions of the shallow landslides. Shallow landslides in the mixed-rock area would occur due to fully saturated cohesive soil layers of more than 2 m thick. Most of these landslides required specific source areas with one to two orders of magnitude larger

than those in the granite area. Impermeable clay-rich layers played a role in sliding surface for some landslide scarps in the mixed-rock area. The triggering conditions of landslides must involve diverse factors, especially in the mixed-rock area where groundwater discharge might intensely influence the slope stability.

Acknowledgments

We thank Jung Hsuan Lin, Hikaru Mura, Naoya Hiramoto and Ryuya Kodama for assistance in field work. The 1-m DEMs were offered from Chugoku Regional Development Bureau, MLIT. This work is financially supported by the JSPS Grants-in-Aid for Scientific Research (16K01214 and 19H01371, PI: Hattanji, T.).

References

Iverson, R.M. (2000): Landslide triggering by rain infiltration. *Water Resour. Res.*, **36**, 1897–1910.

Kaibori, M., Ishikawa, Y., Satofuka, Y., Matsumura, K., Nakatani, K., Hasegawa, Y., Matsumoto, N., Takahara, T., Fukutsuka, K., Yoshino, K., Nagano, E., Fukuda, M., Nakano, Y., Shimada, T., Hori, D., Nishikawa, T. (2014): Sediment-related disasters induced by a heavy rainfall in Hiroshima-city on 20th August, 2014. *Jour. Japan. Soc. Erosion Control Eng.*, **67**(4), 49–59. (in Japanese)

Mathewson, C.C., Keaton, J.R., Santi, P.M. (1990): Role of bedrock ground water in the initiation of debris flows and sustained post-flow stream discharge. *Bulletin of the Association of Engineering Geologists*, **27**, 73–83.

Matsushi, Y., Watakabe, T., Tsou, C.Y., Hirata, Y., Chigira, M. (2015): Triggering mechanisms and rainfall threshold of shallow landslides: Cases in the Hiroshima disaster on 20 August 2014. *Annuals of Disas. Prev. Res. Inst., Kyoto Univ.*, **58A**, 24–33. (in Japanese with English abstract)

Ohsaka, O., Tamura, T., Kubota, J., Tsukamoto, Y. (1992): Process study of the soil stratification on weathered granite slopes. *Jour. Japan. Soc. Erosion Control Eng.*, **45**(3), 3–12. (in Japanese with English abstract)

Onda, Y., Komatsu, Y., Tsujimura, M., Fujihara, J. (2001): The role of subsurface runoff through bedrock on storm flow generation. *Hydrol. Process.*, **15**, 1693–1706.

Onda, Y., Tsujimura, M., Fujihara, J., Ito, J. (2006): Runoff generation mechanisms in high-relief mountainous watersheds with different underlying geology. *Jour. Hydrol.*, **331**, 659–673.

Onda, Y., Tsujimura, M., Tabuchi, H. (2004): The role of subsurface water flow paths on hillslope hydrological processes, landslides and landform development in steep mountains of Japan. *Hydrol. Process.*, **18**, 637-650.

Saito, M., Kawabata, D., Sato, D., Doshida, S., Araiba, K. (2015): Geology of the area where debris flows occurred by a heavy rainfall in Hiroshima at August 20, 2014. *Jour. Geol. Soc. Japan*, **121**, 339–346. (in Japanese with English abstract)

Skempton, A.W., DeLory, F.A. (1957): Stability of Natural Slopes in London Clay. *Proc. 4th Int. Conf. Soil Mech. Found. Eng.*, **2**. 378–381.

Takahashi, Y. (1991): Geology of the Hiroshima district. With Geological Sheet Map at 1:50,000. *Geol. Surv. Japan.* (in Japanese with English abstract)

Wakatsuki, T., Matsukura, Y. (2008): Lithological effects in soil formation and soil slips on weathering-limited slopes underlain by granitic bedrocks in Japan. *Catena*, **72**, 153–168.

Watakabe, T. and Matsushi, Y. (2019): Lithological controls on hydrological processes that trigger shallow landslides: Observations from granite and hornfels hillslopes in Hiroshima, Japan. *Catena*, **180**, 55–68.

Yamashita, K., Hattanji, T., Tanaka, Y., Doshida, S., Matsushima, T. (2017): Topographic characteristics of rainfall-induced shallow landslides on granitic hillslopes: A case study in Hofu City, Yamaguchi Prefecture, Japan. *Tsukuba Geoenvironmental Sciences*, **13**, 23–29.

Received 2 September, 2020
Accepted 5 November, 2020